Published in final edited form as:
Clin Exp Metastasis. 2013 June ; 30(5): 615–630. doi:10.1007/s10585-013-9565-x.

Leading malignant cells initiate collective epithelial cell invasion in a three-dimensional heterotypic tumor spheroid model

Shawn P. Carey[1,*], **Alina Starchenko**[1,*], **Alexandra L. McGregor**[1], and **Cynthia A. Reinhart-King**[1]

[1]Department of Biomedical Engineering, Cornell University, Ithaca, New York, 14853, USA

Abstract

Solid tumors consist of genetically and phenotypically diverse subpopulations of cancer cells with unique capacities for growth, differentiation, and invasion. While the molecular and microenvironmental bases for heterogeneity are increasingly appreciated, the outcomes of such intratumor heterogeneity, particularly in the context of tumor invasion and metastasis, remain poorly understood. To study heterotypic cell-cell interactions and elucidate the biological consequences of intratumor heterogeneity, we developed a tissue-engineered multicellular spheroid (MCS) co-culture model that recapitulates the cellular diversity and fully three-dimensional cell-cell and cell-matrix interactions that characterize human carcinomas. We found that "invasion-competent" malignant cells induced the collective invasion of otherwise "invasion-incompetent" epithelial cells, and that these two cell types consistently exhibited distinct leader and follower roles during invasion. Analysis of extracellular matrix microarchitecture revealed that malignant cell invasion was accompanied by extensive extracellular matrix remodeling including matrix alignment and proteolytic track-making. Inhibition of cell contractility- and proteolysis-mediated matrix reorganization prevented leader-follower behavior and malignant cell-induced epithelial cell invasion. These results indicate that heterogeneous subpopulations within a tumor may possess specialized roles during tumor progression and suggest that complex interactions among the various subpopulations of cancer cells within a tumor may regulate critical aspects of tumor biology and affect clinical outcome.

Keywords

Intratumor heterogeneity; Invasion; Migration; 3D co-culture; Extracellular matrix

Introduction

The tumor microenvironment contains a complex mixture of normal epithelial cells, highly heterogeneous malignant cells, stromal cells, and extracellular matrix (ECM) whose interactions are critical to cancer progression [1, 2]. Despite advances in *in vitro* models that have refined our understanding of how the cellular and noncellular components of the tumor microenvironment cooperate to promote or suppress disease, many tissue-engineered tumor models fail to accurately recapitulate the intratumor heterogeneity and three-dimensional tissue architecture that characterize human carcinomas [3–5]. Notably, biophysical and biochemical interactions among dissimilar cell types within the tumor microenvironment

Corresponding author: Cynthia A. Reinhart-King, 302 Weill Hall, Ithaca, NY 14853, Tel: (607) 255-8491, Fax: (607) 255-7330, cak57@cornell.edu.
*These authors contributed equally to this work.

Conflict of Interest
The authors declare that they have no conflict of interest.

enable many key features of developing cancer including abnormal cell growth [6], enhanced angiogenesis [7], and tissue invasion and metastasis [8–10]. However, the importance of interactions among dissimilar cells *within* the tumor compartment remains to be determined. To better understand how a tumor's constituents cooperate to regulate critical phases of tumor progression, these processes should be studied using well-controlled *in vitro* tumor models that permit three-dimensional, *in vivo*-like interactions among the diverse cells and ECM that comprise the microenvironment.

Since cancer cells continually interact with other cells that are resident within or recruited to the tumor microenvironment, several experimental models have coupled malignant cells with cells such as stromal fibroblasts, endothelial cells, and immune cells to study the underlying mechanisms and clinically-relevant outcomes of heterotypic cell-cell interactions. For example, Gaggioli et al observed that stromal fibroblasts produce cell contractility- and proteolysis-dependent tracks within the ECM that are sufficient to induce squamous cell carcinoma invasion [8]. Additionally, activation of stromal fibroblasts by gastric cancer cells induces stromal expression of pro-angiogenic factors resulting in increased tumor vascularization [7]. Importantly, the cellular diversity of the tumor microenvironment is not limited to these distinct cell types, as cells of epithelial lineage within carcinomas exist along a spectrum ranging from normal epithelial cells to highly variable malignant cells [11]. In addition to the significant heritable diversity that neoplastic cells can exhibit due to the acquisition of genetic and epigenetic alterations during oncogenesis [12], cancer cells exhibit phenotypic plasticity, whereby a cell's genetic program is integrated with biochemical and biophysical cues from the extracellular microenvironment to regulate cellular phenotype [13–15]. The resulting cellular diversity within the epithelial compartment itself gives rise to substantial morphological, physiological, and behavioral intratumor heterogeneity whose functional consequences are poorly understood.

While it is clear that human carcinomas contain subpopulations of cancer cells with unique capacities for growth, differentiation, tissue invasion, and secondary tumor initiation [11, 12], the significance of interactions among cells in these various subgroups are unknown. Since local tissue invasion is both the first discernible step of metastasis and the basis for histopathological diagnosis of metastatic cancer, the invasive potential of tumor cells is of particular clinical relevance [16, 17]. During invasion, cancer cells physically dissociate from the primary tumor mass, bypass the epithelial basement membrane to move from the epithelial compartment into the stromal compartment, and negotiate the three-dimensional interstitial microenvironment on their way to a secondary site [18]. Migration through the three-dimensional stroma requires specialized cellular mechanisms including proteolysis- and cell contractility-based matrix remodeling to overcome steric hindrance imposed by the extracellular matrix [19–22]. Tissue invasion is dependent upon cells' invasive fitness as well as cell-cell and cell-matrix interactions [13, 23]. For example, 3D extracellular matrix microarchitecture [24], alignment [25], and mechanics [26] regulate 3D migration efficiency [27]. Biophysical cell-cell and cell-matrix interactions including cell-cell adhesions and proteolytic matrix patterning provide additional control over the nature of invasion [13, 21, 22, 28]. Together, these findings have established important roles for extracellular control of invasion, but there remains a need to investigate cancer invasion in a more physiologically relevant heterogeneous cancer model where only a subset of cancer cells within a heterogeneous tumor may be "invasion-competent".

Tissue engineering approaches to cancer research have emerged as valuable intermediates between traditional 2D *in vitro* cell culture techniques, which often fail to accurately represent the microenvironmental complexity of tumors, and *in vivo* cancer models, whose extensive complexity can limit experimental control and confound findings [5, 29, 30].

Tissue-engineered platforms such as multicellular spheroids (MCS) incorporate cells and ECM in a three-dimensional physiological context, and thus, are able to effectively recapitulate tumor architecture and cancer cell function, which are coupled through regulation of cell-cell and cell-ECM interactions [31–33]. Thus, tumor spheroids have been widely used to investigate tumorigenesis [34], cellular mechanisms of cancer invasion [20, 35], and anticancer drug efficacy [36]. Importantly, MCS can be made to contain multiple cell types in co-culture and can be dynamically and quantitatively analyzed with confocal microscopy, making them an ideal experimental model with which to explore the functional importance of intratumor heterogeneity.

In this study, we investigated cancer invasion in the framework of intratumor heterogeneity using a tissue-engineered co-culture tumor model in which two dissimilar cell types derived from the epithelial compartment were incorporated into heterotypic multicellular spheroids. Co-culture MCS composed of the “invasion-competent” breast adenocarcinoma cell line MDA-MB-231 and the “invasion-incompetent” breast epithelial cell line MCF-10A were embedded within 3D collagen matrices that permitted *in vivo*-like cell-cell and cell-matrix interactions and, thus, supported physiological *in vitro* tumor progression. Using this co-culture platform, we found that invasive malignant cells induced and led collective invasion of otherwise non-invasive epithelial cells, and that this leader-follower co-invasive behavior was dependent upon cell contractility- and proteolysis-based ECM remodeling by leading malignant cells.

Materials and Methods

Cell culture and reagents

Malignant MDA-MB-231 breast adenocarcinoma cells (HTB-26; ATCC, Rockville, MD) were maintained in DMEM (Invitrogen, Carlsbad, CA) supplemented with 10% fetal bovine serum (Atlanta Biologicals, Norcross, GA) and 1% penicillin-streptomycin (Invitrogen). MDA-MB-231/GFP cells (AKR-201; Cell Biolabs, San Diego, CA) were maintained in complete MDA-MB-231 media supplemented with 0.1mM MEM Non-Essential Amino Acids (Invitrogen). MCF-10A mammary epithelial cells (CRL-10317; ATCC) and MCF-10CA1a malignant mammary epithelial cells (Barbara Ann Karmanos Cancer Institute, Detroit, MI) were maintained in DMEM:F12 (Invitrogen) supplemented with 5% horse serum (Invitrogen), 0.5 $\mu g\ ml^{-1}$ hydrocortisone (Sigma-Aldrich, St. Louis, MO), 20 $ng\ ml^{-1}$ hEGF (Invitrogen), 10 $\mu g\ ml^{-1}$ insulin (Sigma-Aldrich), 100 $ng\ ml^{-1}$ cholera toxin (Sigma-Aldrich), and 1% penicillin-streptomycin. PC-3 malignant prostate adenocarcinoma cells (CRL-1435; ATCC) were maintained in Ham’s F-12K Medium (ATCC) supplemented with 10% fetal bovine serum and 1% penicillin-streptomycin. PrEC primary human prostate epithelial cells (CC-2555; Lonza, Walkersville, MD) were maintained in PrEGM prostate epithelial cell growth medium (Lonza) supplemented with SingleQuots (Lonza) according to the manufacturer’s recommended protocol. Mammary spheroid formation media consisted of complete MCF-10A media supplemented with 0.25% methylcellulose (H4110; StemCell Technologies, Vancouver, BC). Mammary spheroid growth media consisted of complete MCF-10A media supplemented with 0.25% methylcellulose and 1% Matrigel (BD; San Jose, CA). Prostate spheroid formation media consisted of complete PrEC media supplemented with 0.25% methylcellulose. Prostate spheroid growth media consisted of complete PrEC media supplemented with 0.25% methylcellulose and 1% Matrigel. All cell culture was maintained at 37°C and 5% CO_2.

At least 2 h prior to spheroid generation, epithelial cells (MCF-10A, PrEC) and malignant cells (MDA-MB-231, MCF-10CA1a, PC-3) were labeled with 10 μM CellTracker Orange CMRA (Invitrogen) and 10 μM Cell Tracer Green CMFDA SE (Invitrogen), respectively.

GM6001 (EMD Millipore, Billerica, MA) and Y27632 (Sigma-Aldrich) were used at 20 μM and 10 μM, respectively.

Multicellular spheroid generation

To generate multicellular spheroids, fluorescently-labeled cells were trypsinized as for cell passage and resuspended in spheroid formation media at 2.5×10^4 cells ml^{-1}. To prepare epithelial and malignant monoculture spheroids, 200 μl of the appropriate cell suspension (5×10^3 cells) was seeded into each well of non-adhesive round-bottom 96-well plates (Corning; Tewksbury, MA). For epithelial/malignant co-culture spheroids, volumetric mixtures of each cell suspension were seeded into each well. Plates were centrifuged at 1000 rpm for 5 min and then incubated at 37°C and 5% CO_2 on an orbital shaker at ~60 rpm for 2 h. Spheroid formation media was then replaced with spheroid growth media to promote spheroid compaction.

3D spheroid invasion assay

After 48 h of compaction, spheroids were embedded in 1.5 mg ml^{-1} and 6.0 mg ml^{-1} type I collagen gels. Collagen gels were prepared as previously described [24]. Briefly, type I collagen was acid-extracted from rat tail tendons (Pel-Freez Biologicals, Rogers, AR), purified via centrifugation and lyophilization, and reconstituted at 10 mg ml^{-1} in 0.1% acetic acid. Stock collagen solution was diluted to either 1.5 mg ml^{-1} or 6.0 mg ml^{-1} by gently mixing with ice-cold DMEM, and the solution was neutralized to pH 7.0 with 1N NaOH. Spheroids were removed from culture plates and individually embedded within 500 μl collagen gels in glass-bottom 24-well plates (MatTek, Ashland, MA). After 30 minutes of gel polymerization at 37°C, gels were overlaid with 500 μl of complete MCF-10A or PrEC media with or without pharmacological inhibitors.

Microscopy and image analysis

Real-time spheroid compaction and invasion were measured with time-lapse microscopy using a Zeiss AxioObserver Z1 inverted phase contrast microscope equipped with a Hamamatsu ORCA-ER camera. For compaction analysis, spheroids were imaged at 2-h intervals for 24 h in a temperature-, humidity-, and CO_2-controlled microscope incubation chamber using AxioVision software (v. 4.8, Carl Zeiss MicroImaging GmbH, Jena, Germany). Spheroid cross-sectional area was measured using ImageJ (v. 1.43u, National Institute of Health, Bethesda, MD) and normalized to initial cross-sectional area for $n \geq 10$ spheroids per condition from at least three independent experiments. Simultaneous fluorescence and phase time-lapse microscopy (imaged at 20-min intervals for 24 h) were used to observe invasion of fluorescently-labeled MDA-MB-231 and MCF-10A cells from co-culture mammary spheroids into 1.5 mg ml^{-1} collagen matrices.Intra-spheroid cell organization and spheroid invasion were imaged using a Zeiss LSM700 confocal microscope operated by ZEN software (v. 2010, Carl Zeiss). Low-power (5× and 10×) fluorescent images of spheroids presented herein are maximum intensity z-projections of confocal image stacks acquired from the bottom surface of the spheroid to the spheroid center. Spheroid invasion was calculated by measuring the projected spheroid area immediately after collagen embedding (A_0) and the projected spheroid area following culture within collagen matrix for 48 h (A_{Inv}). Invasive Index was defined as $(A_{Inv}/A_0) - 1$ for $n \geq 10$ spheroids per condition from at least three independent experiments. Maximal invasion distance was determined by measuring the radial distance (in μm) from the spheroid edge to the invasive cells furthest from the spheroid for $n \geq 10$ spheroids per condition (four cells measured per spheroid) from at least three independent experiments. To further investigate invasion from co-culture mammary spheroids, the number of epithelial cell-containing invasive strands per spheroid was quantified for $n \geq 10$ co-culture spheroids after 48 h of invasion.

For E-cadherin immunofluorescence, mammary spheroids composed of MDA-MB-231/GFP and unlabeled MCF-10A cells were embedded in 1.5 mg ml^{-1} collagen and either fixed immediately or allowed to invade for 48 h before fixation. Briefly, samples were fixed with 3.7% (v/v) formaldehyde in PBS, permeabilized with 1% (v/v) Triton (JT Baker, Phillipsburg, NJ) in PBS, and blocked with 0.5% (v/v) Tween (JT Baker) with 3% (w/v) bovine serum albumin (Sigma-Aldrich) in PBS. An anti-E-Cadherin primary antibody (sc-7870; Santa Cruz Biotechnology Inc., Santa Cruz, CA) was used at (1:50) in 1% (w/v) BSA in PBS and an Alexa Fluor 568 conjugated secondary antibody (Santa Cruz) was used at (1:100) in 1% (w/v) BSA. Nuclei were stained with 4,6-diamidino-2-phenylindole (DAPI; Sigma-Aldrich).

Cell localization/immunofluorescence and collagen fiber organization before and during spheroid invasion were assessed with high-power (40×) fluorescence and reflectance confocal microscopy, respectively. Confocal reflectance images of collagen fibers are 1-μm thick confocal slices acquired as previously described near the spheroid "equator" [24]. The ImageJ plugin OrientationJ was used as previously described to measure collagen fiber orientation from confocal reflectance images [37]. Grayscale confocal reflectance images of collagen fibers were analyzed and colorized with OrientationJ such that pixel hue corresponded to the angle of local fiber orientation, which could range from −90° to +90° relative to horizontal. To quantify collagen fiber organization, collagen fiber angle (θ_{Fiber}) relative to the tangent of the original spheroid surface (θ_{Sph}) was determined for each pixel in the given region of interest using the algorithm $|\theta_{Fiber} - \theta_{Sph}|$. Using this analysis, the minimum angular difference was 0°, which corresponded to a tangentially-aligned fiber; the maximum angular difference was 90°, which corresponded to a radially-aligned fiber. Results are graphed as frequency distributions of the angular difference, binned in 10-degree increments, between collagen fibers and the spheroid surface for all pixels within the indicated regions of interest.

Statistical analysis

Data was compared by one-way analysis of variance (ANOVA) with post-hoc Tukey HSD tests using JMP Pro software (v. 9.0.2, SAS Institute, Cary, NC). All numeric data is presented as mean ± SE; statistical significance was considered with $p < 0.01$.

Results

Multicellular spheroid generation and characterization

To experimentally recapitulate intratumor heterogeneity and study heterogeneity-associated phenomena, a multicellular spheroid model was developed. Fluorescently-labeled epithelial cells (labeled red) and malignant cells (labeled green) were seeded in round-bottom 96-well plates (Fig. 1a; 0 h) and allowed to spontaneously coalesce and compact over 24 h to form multicellular spheroids (Fig. 1a; insets). Fluorescence confocal microscopy and transmitted light microscopy were used to probe cellular distribution and spheroid morphology, respectively. MCF-10A epithelial monoculture spheroids were densely-compacted, while MDA-MB-231 malignant monoculture spheroids were more loosely aggregated. Co-culture spheroids (1:1 mixture of MCF-10A cells and MDA-MB-231 cells) exhibited intermediate compaction (Fig. 1a; 24 h). Tracking of spheroid area over 24 h showed that spheroid compaction, and thus, final spheroid size, was dependent on cellular composition (Fig. 1b). Purely epithelial spheroids compacted rapidly and had final cross-sectional areas of 16.9 ± 0.8% of the initial cell pellet. Co-culture spheroids compacted more slowly and had final cross-sectional areas of 19.9 ± 0.5% of the initial cell pellet. Purely malignant spheroids exhibited slower compaction than spheroids containing epithelial cells and had cross-sectional areas of 28.4 ± 2.1 % of the initial cell pellet.

While epithelial and malignant monoculture spheroids contained homogeneous cellular distributions, epithelial/malignant co-culture spheroids contained clusters of each cell type. Confocal microscopy showed that these cell clusters were organized into distinct regions of the spheroid (Fig. 2a). Consistently, a core of malignant cells was encased in a shell of epithelial cells (Fig. 2a; 100–125 μm), which was surrounded by an outer layer of malignant cells (Fig. 2a; all slices). Time-lapse fluorescence microscopy demonstrated that malignant cells peripheral to the epithelial shell were highly motile at the conclusion of compaction (Fig. 2b). E-cadherin was localized to MCF-10A cell membranes (Fig. 2c; white arrowheads), but absent from fluorescently-labeled MDA-MB-231 cells (Fig. 2c; black arrowheads) in co-culture spheroids.

Three-dimensional multicellular spheroid invasion

To examine invasion from multicellular spheroids in a 3D physiological context, fluorescently-labeled spheroids were fully embedded within collagen gels and imaged immediately and after 48 h. During this culture period, MCF-10A epithelial cells in monoculture spheroids remained non-invasive (Fig. 3a), with these spheroids only undergoing some non-invasive expansive growth, as indicated by a small non-zero Invasive Index of 0.22 ± 0.04 (Fig. 3b) and no detectable Maximal Invasion Distance (Fig. 3c). In contrast, MDA-MB-231 malignant cells at the periphery of both epithelial/malignant co-culture and malignant monoculture spheroids extended exploratory cell protrusions and began to invade the matrix within 3 h after collagen embedding. After 48 h, co-culture and MDA-MB-231 malignant spheroids showed extensive collagen invasion (Fig. 3a), resulting in statistically significant Invasive Indices of 2.3 ± 0.1 and 3.6 ± 0.2, respectively (Fig. 3b). Cells invading from these spheroids exhibited statistically equivalent Maximal Invasion Distances of 276 ± 13 μm and 296 ± 14 μm, respectively (Fig. 3c). MDA-MB-231 malignant cells (labeled green) invaded readily in a disorganized manner from both co-culture and malignant spheroids. Notably, when cultured with malignant cells in co-culture spheroids, normally non-invasive MCF-10A epithelial cells (labeled red) became invasive (Fig. 3a; arrowheads). Examination of cells invading from co-culture spheroids revealed that invading epithelial cells (Fig. 4a; black arrowheads) were consistently organized in invasive strands that were led by one or more leading malignant cells (Fig. 4a; white arrowheads). Another malignant mammary cell type, MCF-10CA1a, was similarly able to induce invasion of MCF-10A epithelial cells (Fig. 4b). Further, PC-3 malignant prostate adenocarcinoma cells induced invasion of otherwise non-invasive (data not shown) PrEC primary prostate epithelial cells (Fig. 4c). In each of these systems, malignant cells (MDA-MB-231, MCF10CA1a, or PC-3) were positioned at the tip of invasive strands (Fig. 4a–c, white arrowheads) and epithelial cells (MCF-10A or PrEC) were trailing behind (Fig. 4a–c, black arrowheads).

Extracellular matrix remodeling during spheroid invasion

To more closely examine the differential invasion observed from multicellular spheroids, confocal fluorescence and reflectance microscopy were used to probe cell localization and extracellular matrix organization at the spheroid-matrix interface, respectively. Immediately following collagen embedding, all spheroids were surrounded by uniform collagen matrices containing randomly organized fibers (Fig. 5a; 0 h). After 48 h, collagen fiber reorganization and alignment were observed in all conditions (Fig. 5a; 48 h, white arrowheads) as compared to naïve matrices at 0 h. The non-invasive expansive growth exhibited by MCF-10A epithelial spheroids was accompanied by reorganization of collagen fibers tangential to the spheroid surface such that fibers were wrapped around the spheroid (Fig. 5a; 48 h). Quantitative analysis of fiber alignment using OrientationJ confirmed that the fibers in the indicated region of interest were preferentially aligned parallel to the epithelial spheroid surface, as shown by a small difference between θ_{Fiber} and θ_{Sph} (Fig. 5b;

MCF-10A). Confocal imaging revealed that cellular invasion from epithelial/malignant co-culture and MDA-MB-231 malignant monoculture spheroids was associated with remodeling of collagen fibers perpendicular to the spheroid surface (Fig. 5a; 48 h). Quantification of ECM alignment in the proximity of invading cells with OrientationJ verified that collagen fibers were oriented orthogonal to the spheroid surface, as indicated by relatively large differences between θ_{Fiber} and θ_{Sph} (Fig. 5b; Co-culture and MDA-MB-231). Consistently, leading malignant cells were elongated and radially-oriented. Malignant and epithelial following cells tended to show rounded morphologies, with the latter forming cohesive invasive strands. Notably, invading malignant MDA-MB-231 leader cells left cell-scale microtracks in the matrix behind them, as indicated by regions of high collagen reflectance surrounding regions devoid of extracellular matrix (Fig. 5a; 48 h, black arrowheads in cross-section inset). Time-lapse imaging revealed the time-course and dynamics of invasion from co-culture spheroids and showed that leading malignant MDA-MB-231 cells persisted at the tips of invasive strands (Fig. 6a; white arrowheads). Importantly, co-invasion was maintained even when transient gaps (Fig. 6a; black arrowheads) formed between leading MDA-MB-231 cells and following MCF-10A cells. Together, time-lapse imaging and confocal microscopy (Fig. 6b) showed that trailing epithelial cells exhibited two general induced-invasion strategies: (i) MCF-10A cells fill matrix tunnels (Fig. 6b; black arrowheads) left by invading MDA-MB-231 cells; and (ii) MCF-10A cells invade directly behind and adjacent to leading MDA-MB-231 cells. E-cadherin was consistently detected between following MCF-10A epithelial cells (Fig. 6b,c; white arrowheads), but not in leading MDA-MB-231 cells or between adjacent MDA-MB-231 cells (Fig. 6c,d).

Since fiber reorganization and proteolytic track-making were associated with cell invasion and malignant MDA-MB-231 cells consistently led invasive strands of epithelial MCF-10A cells during invasion from co-culture spheroids, we hypothesized that extracellular matrix remodeling by leading malignant cells was required for 3D invasion from multicellular spheroids. To test this hypothesis, co-culture spheroids were embedded within 1.5 mg ml^{-1} collagen matrices and treated with GM6001 (20 μM) to inhibit MMP activity or Y-27632 (10 μM) to inhibit ROCK-based cell contractility. Confocal reflectance imaging around invading cells at the spheroid-matrix interface showed that collagen fiber alignment and matrix microtracks, which were prominent in control conditions, were absent under MMP and ROCK inhibition (Fig. 7a; black arrowheads). Quantification of ECM alignment indicated that treatment with GM6001 or Y27632 attenuated the fiber alignment observed in control conditions. Briefly, fibers within control ECM tended to be oriented perpendicular to the spheroid surface (large difference between θ_{Fiber} and θ_{Sph}) while fibers within GM6001- and Y27632-treated matrices showed reduced preferential orientation (Fig. 7c). MDA-MB-231 invasion past the original spheroid boundary (Fig. 8a; dashed white lines) persisted under both MMP and ROCK inhibition (Fig. 8a). However, the extent of invasion was decreased: MMP and ROCK inhibition significantly reduced Invasive Index from 2.3 ± 0.1 to 1.5 ± 0.2 and 1.4 ± 0.2, respectively (Fig. 8c), and significantly reduced Maximal Invasion Distance from 276 ± 13 μm to 217 ± 19 μm and 146 ± 15 μm, respectively (Fig. 8d). Similar trends of reduced invasion under MMP and ROCK inhibition were observed in MDA-MB-231 monoculture spheroid studies (Supplementary Fig. S1). Notably, co-culture spheroids exhibited 9.8 ± 1.5 $MCF\text{-}10A^{+}$ invasive strands per spheroid (Fig. 8a; white arrowheads), but no such epithelial cell-positive invasive strands were observed under MMP or ROCK inhibition (Fig. 8a,e).

To investigate the role of matrix microarchitecture in regulating invasion, co-culture spheroids were embedded within high-density 6.0 mg ml^{-1} collagen matrices. These matrices have a more confined microarchitecture consisting of a tight meshwork of short collagen fibers and small pores (Fig. 7b; inset) as compared to low-density 1.5 mg ml^{-1}

collagen matrices, which contain larger fibers and pores (Fig. 7a; inset). As in low-density gels, matrix remodeling was prominent in control conditions (Fig. 7b; black arrowheads), but was reduced in cultures subjected to MMP or ROCK inhibition, which showed no matrix microtracks and reduced collagen fiber alignment (Fig. 7b,d). Invasion into high-density matrices, as indicated by Invasive Index and Maximal Invasion Distance, was significantly reduced by 55% and 40%, respectively, compared to invasion into low-density matrices under control conditions (Fig. 8c,d); however, matrix density did not change the frequency of MCF-10A$^+$ invasive strands under control conditions (Fig. 8e). Similar to as in low-density matrices, inhibition of MMP or ROCK activity mitigated invasion into high-density matrices (Fig. 8b–d). MMP and ROCK inhibition significantly reduced the Invasive Indices to 0.28 ± 0.04 and 0.35 ± 0.03, respectively, which were close to the Invasive Index exhibited by non-invasive MCF-10A epithelial monoculture spheroids (Fig. 8c; dashed line). Max invasion distance was reduced from 165 ± 10 to 58 ± 7 and 76 ± 6 by MMP and ROCK inhibition, respectively (Fig. 8d). These values are consistent with the observation that malignant cells extended thin protrusions from the spheroid periphery into the matrix, but did not translate completely past the spheroid boundary into the matrix (Fig. 8b; dashed white lines). As in low-density matrix, inhibition of MMP and ROCK activity prevented the development of MCF-10A$^+$ co-invasive strands in 6.0 mg ml^{-1} matrices (Fig. 8b,e).

Discussion

Solid tumors, which initially arise by clonal expansion of transformed cells, contain diverse subpopulations that result from genetic instability, microenvironmental selective pressures, and the reinforcement of enabling phenotypes [12, 38, 39]. Such heritable diversity, when coupled with the phenotypic plasticity that characterizes cancer cells [15], results in substantial intratumor heterogeneity that can obscure the study, diagnosis, and treatment of cancer [4, 40]. To study the functional consequences of such cellular variety in a controlled *in vitro* system, we have developed a tissue-engineered model of intratumor heterogeneity using two dissimilar mammary cell types in co-culture multicellular spheroids. Using this platform, we have established a new model for collective cancer cell invasion in which invasive malignant cells can initiate the invasion of otherwise non-invasive cells within the tumor through cell contractility- and proteolysis-dependent matrix remodeling. To our knowledge, this is the first study that links the distinct leader and follower roles inherent in collective cancer cell invasion to differential invasiveness and intratumor heterogeneity. Thus, this study provides new insight into interactions between cell subpopulations within heterogeneous tumors.

Development and characterization of a fundamental in vitro model of intratumor heterogeneity

To generate a well-defined *in vitro* model of intratumor heterogeneity, co-culture multicellular spheroids were made by mixing equal numbers of fluorescently-labeled cells from two dissimilar mammary cell lines: the malignant breast adenocarcinoma cell line MDA-MB-231 and the breast epithelial cell line MCF-10A. These two cell lines were used throughout this study to represent two discrete subpopulations of cells within a tumor and were chosen because of their distinct invasive/metastatic potentials as well as their considerable historical and scientific significance within the field of breast cancer research. While MCF-10A cells exhibit a more basal phenotype than epithelial cells from normal breast tissue [41], these cells are non-tumorigenic in mice and, because they possess many features of normal mammary epithelial cells, they are extensively used as a model of normal epithelial cells *in vitro* [42, 43]. Malignant and epithelial monoculture spheroids were used throughout the study to demonstrate these cells' behavior in monoculture as a reference. To expand upon the co-culture spheroid system, an alternate malignant mammary epithelial cell

line, MCF-10CA1a, was used in co-culture with MCF-10A epithelial cells. The MCF-10CA1a cell line was derived from a metastatic subpopulation of Ha-ras-overexpressing MCF-10A cells [44]. Further, PC-3 malignant prostate adenocarcinoma cells and PrEC primary prostate epithelial cells were used to investigate intratumor heterogeneity in other tissue systems.

Using the MDA-MB-231 and MCF-10A cell lines, characterization of MCS compaction showed that the rate and extent of spheroid aggregation was dependent upon cell composition. Epithelial MCF-10A spheroids showed the fastest and most extensive compaction while malignant MDA-MB-231 spheroids showed the slowest and least extensive compaction; as expected, co-culture MCF-10A/MDA-MB-231 spheroids exhibited intermediate compaction. These differences in compaction were likely due to differences in the cell-cell and cell-matrix adhesions that participated in aggregation since epithelial cell aggregation is primarily mediated by E-cadherin and malignant cell aggregation is directed by β1 integrin-ECM interactions [45, 46]. Indeed, E-cadherin was only detected on the cell membranes of epithelial MCF-10A cells, and was absent from malignant MDA-MB-231 cells within co-culture spheroids. Such disparity in intercellular adhesiveness is the basis for the differential adhesion hypothesis and, in part, may underlie the cell sorting that was observed in heterotypic co-culture spheroids [47]. Consistently, intermixed cells segregated to form distinct regions of each cell type: a core of malignant cells was encased within a densely-packed shell of epithelial cells, which was surrounded by an outer rim of highly motile malignant cells. The presence of such mobile malignant cells at the spheroid periphery is supported by previous findings [48] and suggests that these cells were actively remodeling their adhesions to reach the physical configuration that maximized adhesion [47]. Consistent with this hypothesis, peripheral malignant cells eventually settled onto and adhered to the spheroid surface. While the specific mechanisms regulating cellular organization within co-culture spheroids remain to be determined, the time course of spheroid formation suggests that differential adhesion and cell sorting, as opposed to proliferation and apoptosis, are responsible for the rapid establishment of cellular organization [49]. An inclusive characterization of the mechanisms governing, and outcomes of, differential cell adhesion, sorting, and survival within heterotypic spheroids was not the aim of this work, and thus, a more comprehensive and rigorous analysis of cell physiology within co-culture spheroids remains an open challenge. Notably, co-culture spheroids can serve as a physiologically-relevant model system within which to study how microenvironmental factors such as cell-matrix interactions, heterotypic cell-cell interactions, and spatially-defined nutrient and growth signals differentially influence cell behaviors relevant to cancer progression [50].

Physiological 3D invasion from an in vitro model of intratumor heterogeneity

Intratumor heterogeneity is thought to have considerable biological and clinical implications due to vast differences in growth, invasive, and differentiation potential among a tumor's cells [4, 11]. During tissue invasion, which is one of the earliest rate-limiting steps of metastasis, malignant cells must spatially and temporally coordinate proteolysis with changes in adhesion, contractility, and cell shape to physically disseminate from the primary tumor [16, 18]. Thus, due to the molecular specialization that is required for efficient invasion, we and others have hypothesized that cells within the tumor may possess different capacities for invasion and metastasis based on their phenotypic abilities [17, 51–53]. To test this hypothesis experimentally, malignant and epithelial cell lines were used in co-culture multicellular spheroids to represent cell subpopulations within a tumor having distinct invasive capacities.

When compacted spheroids were embedded into three-dimensional collagen matrices that mimic the *in vivo* tumor stroma [54], MCF-10A cells in monoculture epithelial spheroids

were unable to invade the matrix and instead exhibited some non-invasive expansive growth. While extracellular cues including matrix stiffness [31], cellular density [55], and growth factors [56] can promote an invasive mesenchymal phenotype in MCF-10A cells, cells in monoculture MCF-10A spheroids maintained a non-invasive epithelial phenotype, and thus, these cells represented an “invasion incompetent” subpopulation. Conversely, “invasion-competent” MDA-MB-231 cells in monoculture form malignant spheroids that readily invaded into the surrounding ECM by first extending exploratory cell projections into the matrix and subsequently translating the cell body away from the spheroid. These opposing behaviors, which were expected based on previous work with these cell types in 3D culture [21, 57], validated the physiological relevance of our 3D culture system. When heterotypic co-culture spheroids were embedded into 3D collagen matrix, they initially showed a pattern of invasion similar to malignant monoculture spheroids, with malignant cells promptly invading into the ECM. After 48 h of culture, the extent of invasion as indicated by measurement of the Invasive Index – the normalized area of invasion – was dependent upon the amount of malignant cells in each culture. Assessment of Maximal Invasion Distance revealed that malignant cells in co-culture spheroids are equally as invasive as malignant cells in monoculture malignant spheroids, indicating that epithelial cells did not restrain malignant cells’ invasive capacity in co-culture.

Interestingly, when co-cultured with malignant MDA-MB-231 cells, otherwise non-invasive epithelial MCF-10A cells were triggered to invade into the matrix in cohesive strands following one or more leading malignant cells. This pattern of “co-invasion”, with distinct leader cells and cohesive strands or masses of invading follower cells, is indicative of collective migration, which occurs during development, regeneration, and epithelial cancer invasion [8, 21, 28, 58–60]. An alternate malignant mammary epithelial cell line, MCF-10CA1a, was similarly able to induce and lead invasion of MCF-10A cells and PC-3 malignant prostate cells led invasive strands of normally non-invasive PrEC primary prostate epithelial cells. While there were clear differences in cellular phenotypes and the nature of co-invasion among the cell lines used, the emergence of leader-follower collective invasion and consistent presence of malignant cells at the tips of invasive strands indicate that this phenomenon is not limited to MDA-MB-231/MCF-10A co-cultures. Further, the incidence of leader-follower co-invasion in prostate co-cultures suggests that this behavior extends to other tissue systems and that non-invasive primary cells can be induced to invade by malignant leader cells *in vitro*. Notably, a defining feature of collective cell migration is the preservation of cell-cell adhesions, and thus, an epithelial phenotype, in migrating cells [13, 61]. Here, we found that epithelial follower cells, but not malignant leader cells, retained such cell-cell cohesion when invading from co-culture spheroids. E-cadherin was maintained at cell-cell junctions between adjacent MCF-10A cells both within the spheroid mass and within invasive strands, indicating retention of an epithelial phenotype in co-invading MCF-10A cells. Thus, using our co-culture system, we demonstrate for the first time that the leader and follower roles characteristic of collective cancer invasion can be assumed by two distinct cellular subpopulations within a tumor.

Collective cell migration through physiological three-dimensional matrices requires that matrices contain adequately large pores through which strands or clusters of cells can pass [13]. However, in the present study as well as in many tissues throughout the body [54], cell diameter can exceed ECM pore diameter, thus providing a barrier to 3D migration that requires cell-mediated extracellular matrix remodeling to permit invasion [62]. The concurrence and interdependence of 3D cell invasion and extracellular matrix remodeling has been extensively documented both *in vitro* and *in vivo* [8, 20–22, 25, 63, 64]. Notably, the Weiss group showed that cancer cells use the membrane-anchored proteinase MT1-MMP to cleave collagen and migrate through cross-linked collagen gels *in vitro* and interstitial ECM *in vivo* [22]. In defining the spatiotemporal dynamics of pericellular

proteolysis during 3D invasion, Wolf et al showed that malignant cells migrating through 3D matrices can proteolytically generate tunnel-like cell-scale microtracks that facilitate further cellular infiltration and proteolysis, eventually leading to the formation of macrotracks and the emergence of collective cell invasion [21]. Using a co-culture tumor model, Gaggioli et al showed that cell-contractility and proteolysis-dependent matrix remodeling by stromal fibroblasts can induce the invasion of squamous cell carcinoma cells and that these cancer cells retain an epithelial phenotype as they collectively advance through matrix tunnels left by fibroblasts [8].

In the current study, confocal reflectance microscopy was used to assess the organization of collagen fibers around spheroids embedded within physiological fibrillar matrices. Collagen fibers around invading malignant and co-culture spheroids were preferentially aligned orthogonal to the spheroid surface while fibers surrounding non-invasive epithelial spheroids were aligned tangential to the spheroid surface. Since naïve collagen matrices and matrix far from spheroids consisted of networks of isotropically oriented fibers, these results indicate that local ECM remodeling at the spheroid-matrix interface occurred in all conditions. The circumferential alignment of fibers around non-invasive MCF-10A epithelial spheroids suggests that the growing spheroid applied outward pressure to compress the matrix [65]. Similar matrix alignment was observed in work by Provenzano et al that identified tangentially organized ECM around non-invasive mammary tumors *in vivo* [25]. The radial matrix organization associated with invasion in malignant monoculture and epithelial/malignant co-culture spheroids was due to active cell-mediated ECM remodeling by cells at the spheroid-matrix interface. Since cells in 3D physiological matrices exert traction forces on the ECM that can result in long-range physical changes in the surrounding matrix [66] and fibers up to several hundred microns from invading cells showed radial realignment in our model, we concluded that malignant cells caused cell contractility-mediated matrix reorganization in our system. Previous work has shown that such Rho-ROCK-based cell contractility is required for collagen fiber alignment at the tumor-stroma interface [67]. This alignment promotes contact guidance and invasion *in vivo* [25], and thus, may serve a similar role in our model. Further, invading malignant cells also produced cell-scale microtracks through the matrix as reported elsewhere [21, 22], and in co-culture spheroids, cohorts of epithelial cells infiltrated these microtracks. Such microtracks have been shown to enable non-proteolytic cell infiltration [35, 68]. Notably, E-cadherin was only detected between adjacent following MCF-10A epithelial cells and transient gaps between leading and following cells opened and closed during co-invasion. These results suggest that E-cadherin may be required for cohesive MCF-10A migration but that matrix tunnels, rather than cell-cell adhesions between leading and following cells, enable the induced invasive phenotype. Since we cannot rule out the possibility that malignant and epithelial cells interact using other adhesion molecules [45, 46, 49], future work should further define the mechanisms of leader-follower collective invasion in this system.

The use of cell traction forces and pericellular proteolysis to generate paths of least resistance is a general property of leader cells during three-dimensional collective migration in several systems [21, 60, 69, 70]. To determine if matrix remodeling by leading malignant cells in our co-culture system was required for the development of epithelial cell-positive co-invasive strands, cultures were treated with inhibitors of MMPs (GM6001) and ROCK-mediated cell contractility (Y27632). As expected, these inhibitors prevented the formation of matrix microtracks and quantitatively reduced matrix alignment at the spheroid-matrix interface, validating the efficacy of inhibition. While MMP and ROCK inhibition quantitatively reduced the efficiency of malignant cell invasion in both monoculture MDA-MB-231 and co-culture spheroids, presumably because the repertoire of 3D migration strategies available to cells was limited [71], these treatments completely prevented induced epithelial co-invasion. Together with our matrix remodeling observations, these findings

support the hypothesis that matrix remodeling by leading invasive cancer cells was necessary for the induction of collective invasion by otherwise non-invasive cells.

Previously, we showed that 3D migration of MDA-MB-231 malignant cells is sensitive to matrix microarchitecture [24], so we used high-density 6.0 mg ml^{-1} collagen matrices to investigate the relationship between matrix structure, matrix remodeling, and invasion. Consistent with previous work showing that matrix density negatively correlates with 3D invasion efficiency [21, 24], here, we found that invasion from spheroids was less efficient in high-density matrices. Notably, while MDA-MB-231 cells were able to invade low-density matrix under MMP and ROCK inhibition, malignant cells at the periphery of spheroids embedded in high-density collagen matrix only extended thin protrusions into the surrounding matrix when treated with MMP and ROCK inhibitors, suggesting that high-density collagen matrices, but not low-density matrices, provided a barrier to MMP- and ROCK-independent invasion. The finding that MDA-MB-231 cells within low-density matrices retained their invasive phenotype under MMP and ROCK inhibition is supported by previous work with these cells [67], and suggests that malignant cells were sufficiently deformable to squeeze through the pores in low-density collagen matrices [72]. In support of this hypothesis, we observed that low-density collagen matrices were heterogeneous and contained a wide distribution of pore sizes, including sufficiently large pores that could potentially serve as “pro-invasive” microdomains through which malignant cells could migrate without matrix remodeling. While the absolute requirement for extracellular proteolysis during cell invasion through physiological 3D matrices remains a topic of debate, it is evident that this requirement is dependent upon local physical properties of the matrix (e.g., pore size and the presence of intermolecular crosslinks) that determine the degree to which the matrix serves as a barrier to invasion [20, 22, 73].

ROCK-mediated cell contractility has been shown to serve many functions in three-dimensional cell migration including driving cell deformation for amoeboid movement and the generation of cell tension and strengthening of adhesions for matrix remodeling [67, 74–77]. Interestingly, Sahai and Marshall showed that rounded amoeboid cell motility, but not elongated protrusive movement, has a significant requirement for Rho-ROCK activity [74]. Consistent with this, we found that malignant cells, which adopted an elongated mesenchymal motile phenotype, were still able to invade within permissive low-density matrices under ROCK inhibition. Thus, as previously shown [67], these results suggest that ROCK-mediated contractility was primarily responsible for matrix alignment and remodeling in our system, which acted to enhance, but was not required for, malignant cell invasion. Interestingly, we found that inhibition of force-mediated matrix remodeling prevented the formation of matrix microtracks by malignant cells, and thus, blocked induced MCF-10A invasion in co-cultures. These findings, which are supported by previous work by Gaggioli et al with matrix-remodeling fibroblasts [8], suggest that coordinated proteolytic- and cell force-mediated matrix remodeling were critical for the formation of invasion-inducing microtracks. Indeed, regardless of matrix density, MCF-10A cells were only induced to co-invade when malignant cells were able to both invade into and remodel the surrounding matrix. This co-invasion occurred at the same frequency in low- and high-density matrices, and was similarly associated with extracellular matrix remodeling, suggesting that the ability of leading MDA-MB-231 cells to generate matrix tunnels under control conditions was not sensitive to the matrix densities used in this study.

Our conclusion that proteolytic- and cell force-mediated matrix priming by leading invasive cells promoted the invasion of otherwise non-invasive cells is consistent with previous work in other experimental systems [8, 78]. While the use of global inhibitors of MMPs and ROCK prevents us from definitively ruling out the possibilities that (i) the epithelial follower cells themselves required ROCK and/or MMP activity to invade or that (ii) global

MMP and ROCK inhibition indirectly altered off-target aspects of cell physiology [79], our data and others' suggest that the limiting factor for induced collective epithelial invasion in this model was the efficient generation of matrix tunnels by leading malignant cells. Nonetheless, future work should seek to more selectively down-regulate cell contractility and proteolytic machinery in a cell-type and isoform-specific manner to systematically define the molecular mechanisms required for leader-follower collective invasion and limit off-target effects.

We propose the following model for malignant cell-induced epithelial cell invasion in our novel heterotypic spheroid system. First, Rho-ROCK-based cell contractility enables ECM alignment by malignant cells that extend into the matrix at the spheroid periphery. This matrix priming facilitates efficient 3D migration of malignant cells into the surrounding matrix, where they can couple their migration with pericellular proteolysis to generate cell-scale microtracks through the ECM. Finally, invasion-incompetent epithelial cells infiltrate matrix tunnels as cohesive strands or clusters of cells, resulting in collective invasion. In this paradigm, ROCK and MMP activity are required for distinct but integrated matrix remodeling functions by leading malignant cells that together lead to efficient generation of matrix tunnels and thus, induced epithelial cell invasion. Our results demonstrate a previously unappreciated instance of intratumor cellular cooperation [4] whereby invasion-competent cancer cells could provide ready-made matrix tunnels to be used by other cells that otherwise lack the ability to invade and negotiate the stromal ECM. In support of this concept, Hanahan and Weinberg recently proposed that, since heterogeneous subpopulations of cells within and around the tumor are likely to be significantly involved in all stages of cancer progression, it is unlikely that progression through the invasion-metastasis cascade is a cell-autonomous process [11]. Further, clear genetic differences have been detected among cells from separate but histologically similar regions of single metastatic tumors [12, 40], suggesting that invasive carcinomas can possess tremendous molecular and phenotypic cellular diversity that remains poorly understood. While the cell types used herein were chosen to represent two tumor subpopulations with distinct invasion capabilities, these results may also give an indication of how malignant cells could affect the remaining non-transformed epithelium within the tumor. Considering the critical role of homotypic epithelial cell-cell interactions in maintaining normal epithelial tissue homeostasis [31, 32], it is conceivable that the heterotypic cell-cell interactions characteristic of heterogeneous tumor cell populations could play a role in promoting the dysfunctional cell behavior and tissue structure observed in invasive carcinomas [80]. Ultimately, the relevance of this *in vitro* model to the metastatic process could be validated *in vivo* to determine if a subpopulation of invasive cells can similarly enable the local invasion, dissemination, and metastasis of otherwise non-invasive cells. Further characterization of heterotypic cell-cell interactions and their functional outcomes within well-defined, tissue-engineered tumor heterogeneity models should provide additional insight into the biological and clinical consequences of intratumor heterogeneity.

Supplementary Material

Refer to Web version on PubMed Central for supplementary material.

Acknowledgments

This work was supported in part by the Cornell Center on the Microenvironment & Metastasis through Award Number U54CA143876 from the National Cancer Institute (NCI) to CAR and a National Science Foundation Graduate Research Fellowship to SPC.

References

1. Bissell MJ, Radisky D. Putting tumours in context. Nat Rev Cancer. 2001; 1:46–54. [PubMed: 11900251]
2. Dvorak HF, Weaver VM, Tlsty TD, Bergers G. Tumor microenvironment and progression. J Surg Oncol. 2011; 103:468–474. [PubMed: 21480238]
3. Fidler IJ. Tumor heterogeneity and the biology of cancer invasion and metastasis. Cancer Res. 1978; 38:2651–2660. [PubMed: 354778]
4. Marusyk A, Polyak K. Tumor heterogeneity: causes and consequences. Biochim Biophys Acta. 2010; 1805:105–117. [PubMed: 19931353]
5. Yamada KM, Cukierman E. Modeling tissue morphogenesis and cancer in 3D. Cell. 2007; 130:601–610. [PubMed: 17719539]
6. Dong-Le Bourhis X, Berthois Y, Millot G, Degeorges A, Sylvi M, Martin P-M, Calvo F. Effect of stromal and epithelial cells derived from normal and tumorous breast tissue on the proliferation of human breast cancer cell lines in co-culture. Int J Cancer. 1997; 71:42–48. [PubMed: 9096664]
7. Guo X, Oshima H, Kitmura T, Taketo MM, Oshima M. Stromal fibroblasts activated by tumor cells promote angiogenesis in mouse gastric cancer. J Biol Chem. 2008; 283:19864–19871. [PubMed: 18495668]
8. Gaggioli C, Hooper S, Hidalgo-Carcedo C, Grosse R, Marshall JF, Harrington K, Sahai E. Fibroblast-led collective invasion of carcinoma cells with differing roles for RhoGTPases in leading and following cells. Nat Cell Biol. 2007; 9:1392–1400. [PubMed: 18037882]
9. Jones JL, Shaw JA, Pringle JH, Walker RA. Primary breast myoepithelial cells exert an invasion-suppressor effect on breast cancer cells via paracrine down-regulation of MMP expression in fibroblasts and tumour cells. J Pathol. 2003; 201:562–572. [PubMed: 14648659]
10. Goswami S, Sahai E, Wyckoff JB, Cammer M, Cox D, Pixley FJ, Stanley ER, Segall JE, Condeelis JS. Macrophages promote the invasion of breast carcinoma cells via a colony-stimulating factor-1/epidermal growth factor paracrine loop. Cancer Res. 2005; 65:5278–5283. [PubMed: 15958574]
11. Hanahan D, Weinberg R. Hallmarks of cancer: the next generation. Cell. 2011; 144(5):646–674. [PubMed: 21376230]
12. Gerlinger M, Rowan A, Horswell S, et al. Intratumor heterogeneity and branched evolution revealed by multiregion sequencing. N Engl J Med. 2012; 366:883–982. [PubMed: 22397650]
13. Friedl P, Wolf K. Plasticity of cell migration: a multiscale tuning model. J Cell Biol. 2010; 188:11–19. [PubMed: 19951899]
14. Provenzano P, Inman D, Eliceiri K, Keely P. Matrix density-induced mechanoregulation of breast cell phenotype, signaling and gene expression through a FAK-ERK linkage. Oncogene. 2009; 28:4326–4343. [PubMed: 19826415]
15. Petersen OW, Lind Nielsen H, Gudjonsson T, Villadsen R, Rønnov-Jessen L, Bissell MJ. The plasticity of human breast carcinoma cells is more than epithelial to mesenchymal conversion. Breast Cancer Res. 2001; 3:213–217. [PubMed: 11434871]
16. Carey SP, D'Alfonso TM, Shin SJ, Reinhart-King CA. Mechanobiology of tumor invasion: engineering meets oncology. Crit Rev Oncol/Hematol. 2012; 83:170–183.
17. Weiss L. Heterogeneity of cancer cell populations and metastasis. Cancer Metastasis Rev. 2000; 19:351–379.
18. Liotta LA, Stetler-Stevenson WG. Tumor invasion and metastasis: an imbalance of positive and negative regulation. Cancer Res. 1991; 51:5054s–5059s. [PubMed: 1884381]
19. Pathak A, Kumar S. Biophysical regulation of tumor cell invasion: moving beyond matrix stiffness. Integr Biol. 2011; 3:267–278.
20. Sabeh F, Shimizu-Hirota R, Weiss SJ. Protease-dependent versus -independent cancer cell invasion programs: three-dimensional amoeboid movement revisited. J Cell Biol. 2009; 185:11–19. [PubMed: 19332889]
21. Wolf K, Wu YI, Liu Y, Geiger J, Tam E, Overall C, Stack MS, Friedl P. Multi-step pericellular proteolysis controls the transition from individual to collective cancer cell invasion. Nat Cell Biol. 2007; 9:893–904. [PubMed: 17618273]

22. Sabeh F, Ota I, Holmbeck K, et al. Tumor cell traffic through the extracellular matrix is controlled by the membrane-anchored collagenase MT1-MMP. J Cell Biol. 2004; 167:769–781. [PubMed: 15557125]
23. Nguyen-Ngoc K-V, Cheung KJ, Brenot A, Shamir ER, Gray RS, Hines WC, Yaswen P, Werb Z, Ewald AJ. ECM microenvironment regulates collective migration and local dissemination in normal and malignant mammary epithelium. Proc Natl Acad Sci USA. 2012; 109:E2595–604. [PubMed: 22923691]
24. Carey SP, Kraning-Rush CM, Williams RM, Reinhart-King CA. Biophysical control of invasive tumor cell behavior by extracellular matrix microarchitecture. Biomaterials. 2012; 33:4157–4165. [PubMed: 22405848]
25. Provenzano PP, Eliceiri KW, Campbell JM, Inman DR, White JG, Keely PJ. Collagen reorganization at the tumor-stromal interface facilitates local invasion. BMC Med. 200610.1186/1741-7015-4-38
26. Levental KR, Yu H, Kass L, et al. Matrix crosslinking forces tumor progression by enhancing integrin signaling. Cell. 2009; 139:891–906. [PubMed: 19931152]
27. Pedersen JA, Swartz MA. Mechanobiology in the third dimension. Ann Biomed Eng. 2005; 33:1469–1490. [PubMed: 16341917]
28. Friedl P, Locker J, Sahai E, Segall JE. Classifying collective cancer cell invasion. Nature Cell Biology. 2012; 14:777–783.
29. Pampaloni F, Reynaud EG, Stelzer EHK. The third dimension bridges the gap between cell culture and live tissue. Nat Rev Mol Cell Bio. 2007; 8:839–845. [PubMed: 17684528]
30. Burdett E, Kasper FK, Mikos AG, Ludwig JA. Engineering tumors: a tissue engineering perspective in cancer biology. Tissue Eng Part B Rev. 2010; 16:351–359. [PubMed: 20092396]
31. Paszek MJ, Zahir N, Johnson KR, et al. Tensional homeostasis and the malignant phenotype. Cancer Cell. 2005; 8:241–254. [PubMed: 16169468]
32. Bissell MJ, Rizki A, Mian IS. Tissue architecture: the ultimate regulator of breast epithelial function. Curr Opin Cell Biol. 2003; 15:753–762. [PubMed: 14644202]
33. Gumbiner BM. Regulation of cadherin-mediated adhesion in morphogenesis. Nat Rev Mol Cell Bio. 2005; 6:622–634. [PubMed: 16025097]
34. Lorenzo C, Frongia C, Jorand R, Fehrenbach J, Weiss P, Maandhui A, Gay G, Ducommun B, Lobjois V. Live cell division dynamics monitoring in 3D large spheroid tumor models using light sheet microscopy. Cell Div. 201110.1186/1747-1028-6-22
35. Ilina O, Bakker G-J, Vasaturo A, Hoffman RM, Friedl P. Two-photon laser-generated microtracks in 3D collagen lattices: principles of MMP-dependent and -independent collective cancer cell invasion. Phys Biol. 2011; 8:015010. [PubMed: 21301056]
36. Pickl M, Ries CH. Comparison of 3D and 2D tumor models reveals enhanced HER2 activation in 3D associated with an increased response to trastuzumab. Oncogene. 2009; 28:461–468. [PubMed: 18978815]
37. Rezakhaniha R, Agianniotis A, Schrauwen J, Griffa A, Sage D, Bouten C, van de Vosse F, Unser M, Stergiopulos N. Experimental investigation of collagen waviness and orientation in the arterial adventitia using confocal laser scanning microscopy. Biomech Model Mechanobiol. 2012; 11:461–473. [PubMed: 21744269]
38. Wolman SR. Cytogenetic heterogeneity: its role in tumor evolution. Cancer Genet Cytogenet. 1986; 19:129–140. [PubMed: 3455660]
39. Nowell PC. The clonal evolution of tumor cell populations. Science. 1976; 194:23–28. [PubMed: 959840]
40. Aubele M, Mattis A, Zitzelsberger H, Walch A, Kremer M, Hutzler P, Höfler H, Werner M. Intratumoral heterogeneity in breast carcinoma revealed by laser-microdissection and comparative genomic hybridization. Cancer Genet Cytogenet. 1999; 110:94–102. [PubMed: 10214356]
41. Keller PJ, Lin AF, Arendt LM, et al. Mapping the cellular and molecular heterogeneity of normal and malignant breast tissues and cultured cell lines. Breast Cancer Res. 2010; 12:R87. [PubMed: 20964822]

42. Debnath J, Muthuswamy SK, Brugge JS. Morphogenesis and oncogenesis of MCF-10A mammary epithelial acini grown in three-dimensional basement membrane cultures. Methods. 2003; 30:256–268. [PubMed: 12798140]
43. Soule HD, Maloney TM, Wolman SR, Peterson WD, Brenz R, Mcgrath CM, Russo J, Pauley RJ, Jones RF, Brooks SC. Isolation and characterization of a spontaneously immortalized human breast epithelial cell line, MCF-10. Cancer Res. 1990; 50:6075–6086. [PubMed: 1975513]
44. Santner S, Dawson P, Tait L, Soule H, Eliason J, Mohamed A, Wolman S, Heppner G, Miller F. Malignant MCF10CA1 cell lines derived from premalignant human breast epithelial MCF10AT cells. Breast Cancer Res Treat. 2001; 65:101–110. [PubMed: 11261825]
45. Ivascu A, Kubbies M. Diversity of cell-mediated adhesions in breast cancer spheroids. Int J Oncology. 2007; 31:1403–1413.
46. Foty RA, Steinberg MS. Cadherin-mediated cell-cell adhesion and tissue segregation in relation to malignancy. Int J Dev Biol. 2004; 48:397–409. [PubMed: 15349815]
47. Foty RA, Steinberg MS. The differential adhesion hypothesis: a direct evaluation. Dev Biol. 2005; 278:255. [PubMed: 15649477]
48. Vamvakidou AP, Mondrinos MJ, Petushi SP, Garcia FU, Lelkes PI, Tozeren A. Heterogeneous breast tumoroids: an in vitro assay for investigating cellular heterogeneity and drug delivery. J Biomol Screen. 2007; 12:13–20. [PubMed: 17166827]
49. Chanson L, Brownfield D, Garbe JC, Kuhn I, Stampfer MR, Bissell MJ, LaBarge MA. Self-organization is a dynamic and lineage-intrinsic property of mammary epithelial cells. Proc Natl Acad Sci USA. 2011; 108:3264–3269. [PubMed: 21300877]
50. Hirschhaeuser F, Menne H, Dittfeld C, West J, Mueller-Klieser W, Kunz-Schughart LA. Multicellular tumor spheroids: an underestimated tool is catching up again. J Biotechnol. 2010; 148:3–15. [PubMed: 20097238]
51. Kraning-Rush CM, Califano JP, Reinhart-King CA. Cellular traction stresses increase with increasing metastatic potential. PloS One. 2012; 7:e32572. [PubMed: 22389710]
52. Liotta LA, Tryggvason K, Garbisa S, Hart I, Foltz CM, Shafie S. Metastatic potential correlates with enzymatic degradation of basement membrane collagen. Nature. 1980; 284:67–68. [PubMed: 6243750]
53. Baker EL, Srivastava J, Yu D, Bonnecaze RT, Zaman MH. Cancer cell migration: integrated roles of matrix mechanics and transforming potential. PloS One. 2011; 6:e20355. [PubMed: 21647371]
54. Wolf K, Alexander S, Schacht V, Coussens LM, von Andrian UH, van Rheenen J, Deryugina E, Friedl P. Collagen-based cell migration models in vitro and in vivo. Semin Cell Dev Biol. 2009; 20:931–941. [PubMed: 19682592]
55. Sarrió D, Rodriguez-Pinilla SM, Hardisson D, Cano A, Moreno-Bueno G, Palacios J. Epithelial-mesenchymal transition in breast cancer relates to the basal-like phenotype. Cancer Res. 2008; 68:989–997. [PubMed: 18281472]
56. Wiercinska E, Naber HPH, Pardali E, van der Pluijm G, van Dam H, ten Dijke P. The TGF-β/Smad pathway induces breast cancer cell invasion through the up-regulation of matrix metalloproteinase 2 and 9 in a spheroid invasion model system. Breast Cancer Res Treat. 2011; 128:657–666. [PubMed: 20821046]
57. Debnath J, Mills KR, Collins NL, Reginato MJ, Muthuswamy SK, Brugge JS. The role of apoptosis in creating and maintaining luminal space within normal and oncogene-expressing mammary acini. Cell. 2002; 111:29–40. [PubMed: 12372298]
58. Alexander S, Koehl G, Hirschberg M, Geissler EK, Friedl P. Dynamic imaging of cancer growth and invasion: a modified skin-fold chamber model. Histochem Cell Biol. 2008; 130:1147–1154. [PubMed: 18987875]
59. Inaki M, Vishnu S, Cliffe A, Rørth P. Effective guidance of collective migration based on differences in cell states. Proc Natl Acad Sci USA. 2012; 109:2027–2032. [PubMed: 22308382]
60. Khalil A, Friedl P. Determinants of leader cells in collective cell migration. Integr Biol. 2010; 2:568–574.
61. Thiery JP. Epithelial-mesenchymal transitions in tumour progression. Nat Rev Cancer. 2002; 2:442–454. [PubMed: 12189386]

62. Friedl P, Wolf K. Tube travel: the role of proteases in individual and collective cancer cell invasion. Cancer Res. 2008; 68:7247–7249. [PubMed: 18794108]
63. Shieh AC, Rozansky HA, Hinz B, Swartz MA. Tumor cell invasion is promoted by interstitial flow-induced matrix priming by stromal fibroblasts. Cancer Res. 2011; 71:790–800. [PubMed: 21245098]
64. Friedl P, Maaser K, Klein CE, Niggemann B, Krohne G, Zänker KS. Migration of highly aggressive MV3 melanoma cells in 3-dimensional collagen lattices results in local matrix reorganization and shedding of alpha2 and beta1 integrins and CD44. Cancer Res. 1997; 57:2061–2070. [PubMed: 9158006]
65. Gordon V, Valentine M, Gardel M, Andor-Ardo D, Dennison S, Bogdanov A, Weitz D, Deisboeck T. Measuring the mechanical stress induced by an expanding multicellular tumor system: a case study. Exp Cell Res. 2003; 289:58–66. [PubMed: 12941604]
66. Kraning-Rush CM, Carey SP, Califano JP, Smith BN, Reinhart-King CA. The role of the cytoskeleton in cellular force generation in 2D and 3D environments. Phys Biol. 2011; 8:015009. [PubMed: 21301071]
67. Provenzano PP, Inman DR, Eliceiri KW, Trier SM, Keely PJ. Contact guidance mediated three-dimensional cell migration is regulated by Rho/ROCK-dependent matrix reorganization. Biophys J. 2008; 95:5374–5384. [PubMed: 18775961]
68. Kraning-Rush CM, Carey SP, Reinhart-King CA. Microfabricated collagen tracks facilitate single cell metastatic invasion in 3D. Integr Biol. 2012
69. De Smet F, Segura I, De Bock K, Hohensinner PJ, Carmeliet P. Mechanisms of vessel branching: filopodia on endothelial tip cells lead the way. Arterioscler Thromb Vasc Biol. 2009; 29:639–649. [PubMed: 19265031]
70. Friedl P, Gilmour D. Collective cell migration in morphogenesis, regeneration and cancer. Nat Rev Mol Cell Bio. 2009; 10:445–457. [PubMed: 19546857]
71. Friedl P, Wolf K. Tumour-cell invasion and migration: diversity and escape mechanisms. Nat Rev Cancer. 2003; 3:362–374. [PubMed: 12724734]
72. Cross SE, Jin Y-S, Rao J, Gimzewski JK. Nanomechanical analysis of cells from cancer patients. Nat Nanotechnol. 2007; 2:780–783. [PubMed: 18654431]
73. Wolf K, Mazo I, Leung H, Engelke K, von Andrian UH, Deryugina EI, Strongin AY, Bröcker E-B, Friedl P. Compensation mechanism in tumor cell migration: mesenchymal-amoeboid transition after blocking of pericellular proteolysis. J Cell Biol. 2003; 160:267–277. [PubMed: 12527751]
74. Sahai E, Marshall CJ. Differing modes of tumour cell invasion have distinct requirements for Rho/ROCK signalling and extracellular proteolysis. Nat Cell Biol. 2003; 5:711–719. [PubMed: 12844144]
75. Wyckoff JB, Pinner SE, Gschmeissner S, Condeelis JS, Sahai E. ROCK- and myosin-dependent matrix deformation enables protease-independent tumor-cell invasion in vivo. Curr Biol. 2006; 16:1515–1523. [PubMed: 16890527]
76. Poincloux R, Collin O, Lizárraga F, Romao M, Debray M, Piel M, Chavrier P. Contractility of the cell rear drives invasion of breast tumor cells in 3D matrigel. Proc Natl Acad Sci USA. 2011; 108:1943–1948. [PubMed: 21245302]
77. Mierke CT, Rösel D, Fabry B, Brábek J. Contractile forces in tumor cell migration. Eur J Cell Biol. 2008; 87:669–676. [PubMed: 18295931]
78. Guiet R, Van Goethem E, Cougoule C, Balor S, Valette A, Al Saati T, Lowell Ca, Le Cabec V, Maridonneau-Parini I. The process of macrophage migration promotes matrix metalloproteinase-independent invasion by tumor cells. J Immunol. 2011; 187:3806–3814. [PubMed: 21880978]
79. Hotary KB, Allen ED, Brooks PC, Datta NS, Long MW, Weiss SJ. Membrane type I matrix metalloproteinase usurps tumor growth control imposed by the three-dimensional extracellular matrix. Cell. 2003; 114(1):33–45. [PubMed: 12859896]
80. Hu M, Yao J, Carroll DK, et al. Regulation of in situ to invasive breast carcinoma transition. Cancer Cell. 2008; 13:394–406. [PubMed: 18455123]

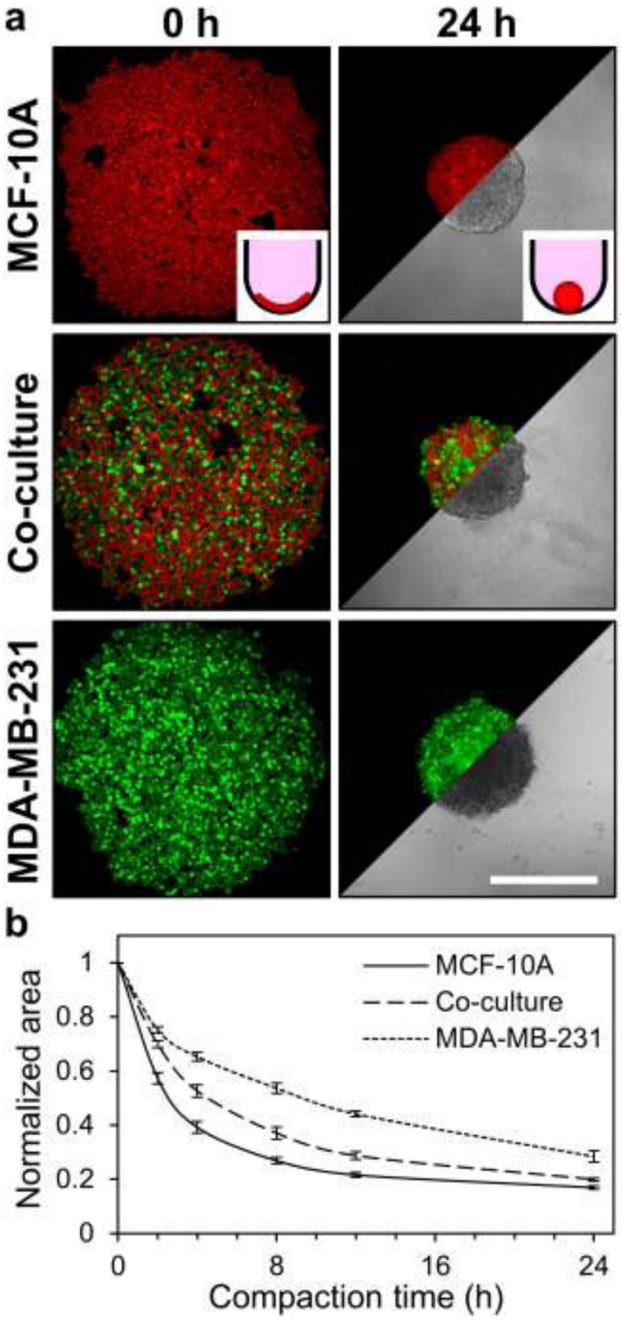

Fig. 1.

Multicellular spheroid compaction. **(a)** Representative confocal fluorescence images (5×) show cell compaction during formation of MCF-10A mammary epithelial cell monoculture (red), MDA-MB-231 malignant breast cell monoculture (green), and MCF10A/MDA-MB-231 co-culture spheroids. Phase images illustrate spheroid morphologies after 24 hours of culture. Insets provide cartoon representation of cells (red) compacting within non-adhesive round-bottom wells to form spheroids. **(b)** Quantification of spheroid cross-sectional area during compaction; data are presented as spheroid cross-sectional area normalized to initial cross-sectional area for n ≥ 11 spheroids from at least three independent experiments. Scale bar = 500 μm

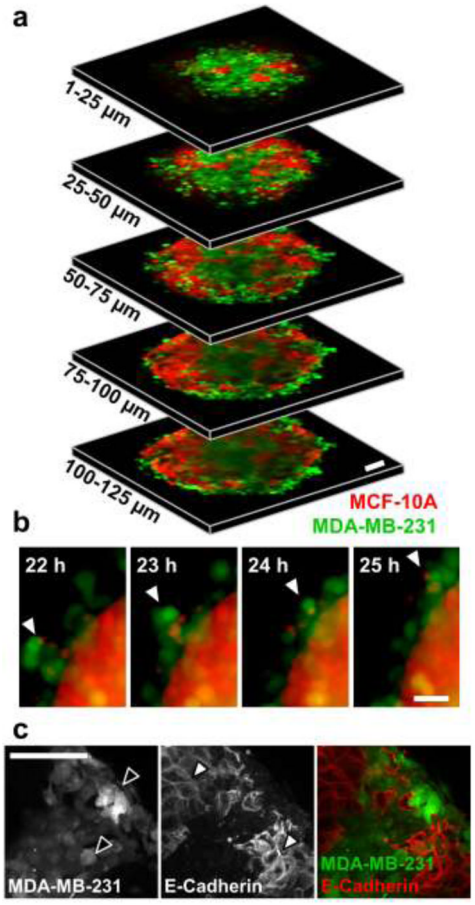

Fig. 2.

Cell organization within heterotypic co-culture spheroids. **(a)** Segmented 25-μm thick z-projections (10×) of co-culture tumor spheroid consisting of fluorescently-labeled MCF-10A (red) and MDA-MB-231 (green) cells after 24 h of compaction highlight localization of two cell types through partial thickness of spheroid. **(b)** Time-lapse imaging at peak spheroid compaction (22–25 h) shows compaction-independent intraspheroid movement of malignant MDA-MB-231 cells. Arrowheads track the movement of a highly-motile cluster of malignant cells that have been excluded to the spheroid periphery. **(c)** Maximum intensity z-projection of co-culture tumor spheroid consisting of fluorescently-labeled MDA-MB-231 and unlabeled MCF-10A cells. Black arrowheads highlight fluorescently-labeled MDA-MB-231 cells and white arrowheads highlight E-cadherin-positive cell membranes of MCF-10A cells. Scale bars = 50 μm

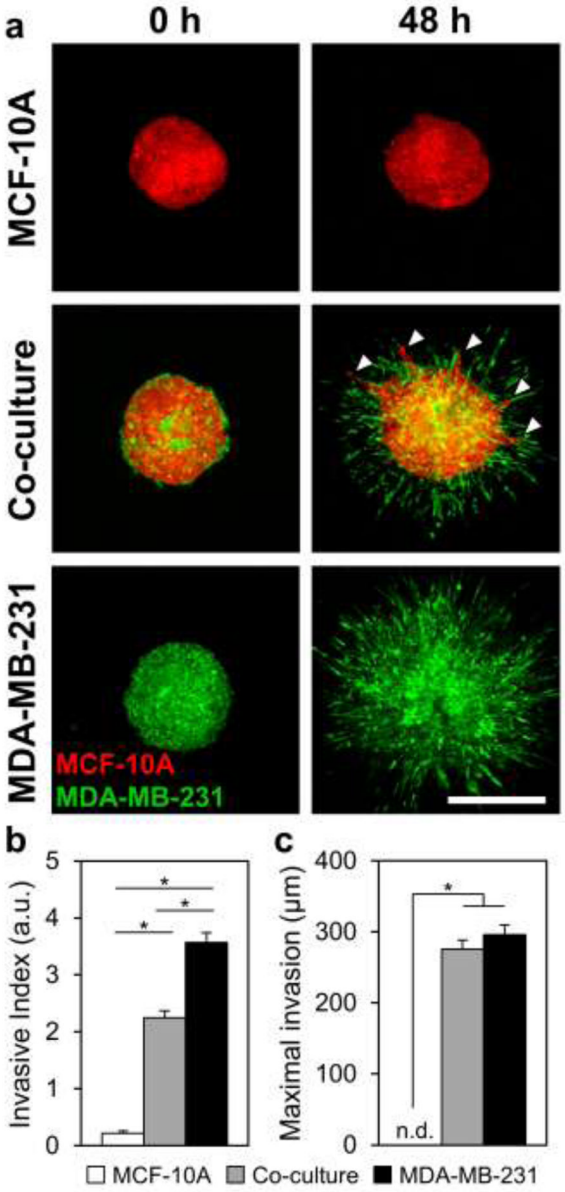

Fig. 3.

Three-dimensional multicellular tumor spheroid invasion. Fluorescently-labeled spheroids were embedded within 1.5 mg ml^{-1} collagen gels and imaged immediately after embedding and at 48 h. **(a)** Representative confocal images (5×) of embedded MCF-10A monoculture, MCF-10A/MDA-MB-231 co-culture, and MDA-MB-231 monoculture spheroids at 0 h and 48 h. Arrowheads indicate strands of epithelial MCF-10A cells invading from co-culture spheroids. **(b)** Quantification of Invasive Index (a.u.) at 48 h; data are presented as spheroid cross-sectional area normalized to initial cross-sectional area at t = 0 h. **(c)** Quantification of maximal invasion distance (μm) at 48 h; data are presented as the radial distance from the spheroid edge to the invasive cells furthest from the spheroid. Data in (b) and (c) are from n ≥ 10 spheroids from at least three independent experiments. Scale bar = 500 μm

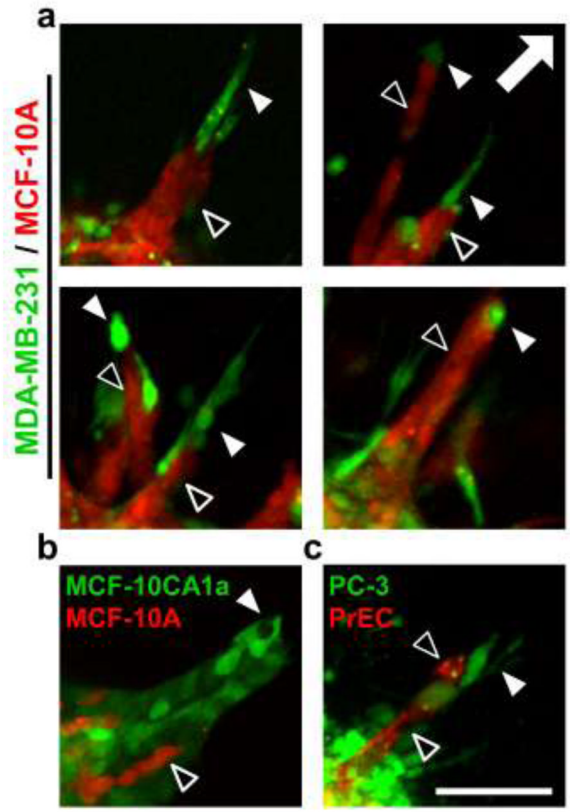

Fig. 4.

Leader-follower behavior in invasive strands. Confocal images (10×) of fluorescently-labeled cells invading into 1.5 mg ml^{-1} collagen matrix from co-culture spheroids demonstrate leading malignant cells (green; white arrowheads) and following epithelial cells (red; black arrowheads). Co-culture combinations include: **(a)** MDA-MB-231 malignant breast adenocarcinoma cells (green) and MCF-10A mammary epithelial cells (red), **(b)** MCF10CA1a malignant mammary epithelial cells (green) and MCF-10A mammary epithelial cells (red), and **(c)** PC-3 malignant prostate adenocarcinoma cells (green) and PrEC primary prostate epithelial cells (red). Arrow indicates direction of invasion away from spheroids, which are in the bottom left corner of each image. Representative images from three independent experiments. Scale bar = 100 μm

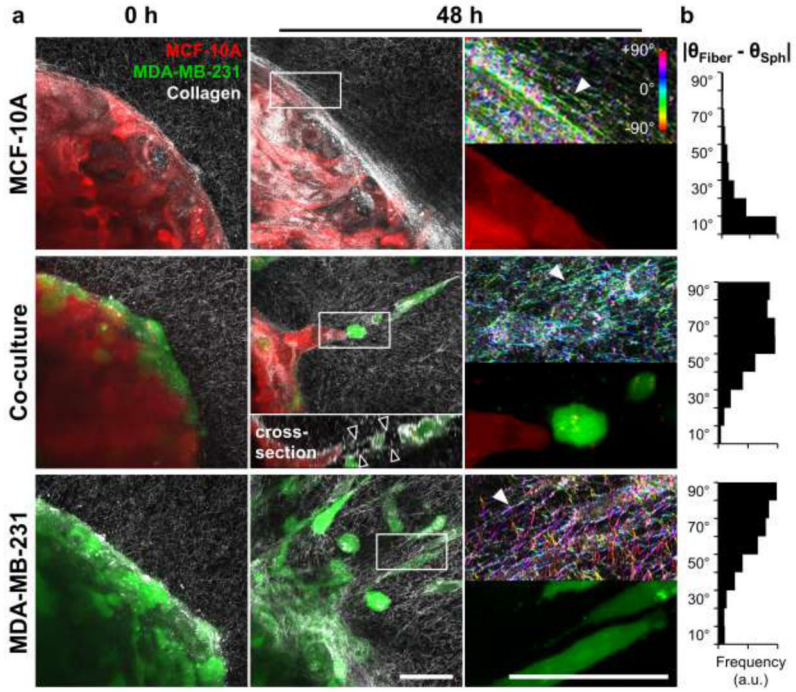

Fig. 5.

Matrix reorganization associated with malignant cell invasion. **(a)** Maximum intensity z-projections (40×) of multicellular tumor spheroids composed of epithelial MCF-10A cells (red) and malignant MDA-MB-231 cells (green), embedded within 1.5 mg ml^{-1} collagen matrix (white fibers imaged by confocal reflectance microscopy) and imaged immediately after embedding (0 h, left panels) and following culture (48 h, middle panels). Regions of interest at 48 h are indicated in middle panels by white boxes and are magnified 3× in right panels. Confocal reflectance images in right panels were colorized with OrientationJ as described in Materials and Methods. White arrowheads highlight areas of collagen fiber alignment. Inset in center panel is cross-sectional view along the invasive strand. Black arrowheads indicate boundaries of matrix microtrack generated by invading malignant leader cells. **(b)** Quantitative analysis of collagen fiber alignment relative to the spheroid surface. Briefly, local collagen fiber orientations (θ_{Fiber}) were determined with OrientationJ and compared to the angle given by the original spheroid surface (θ_{Sph}), resulting in alignment distributions representative of all fibers in the regions of interest. Scale bars = 50 μm

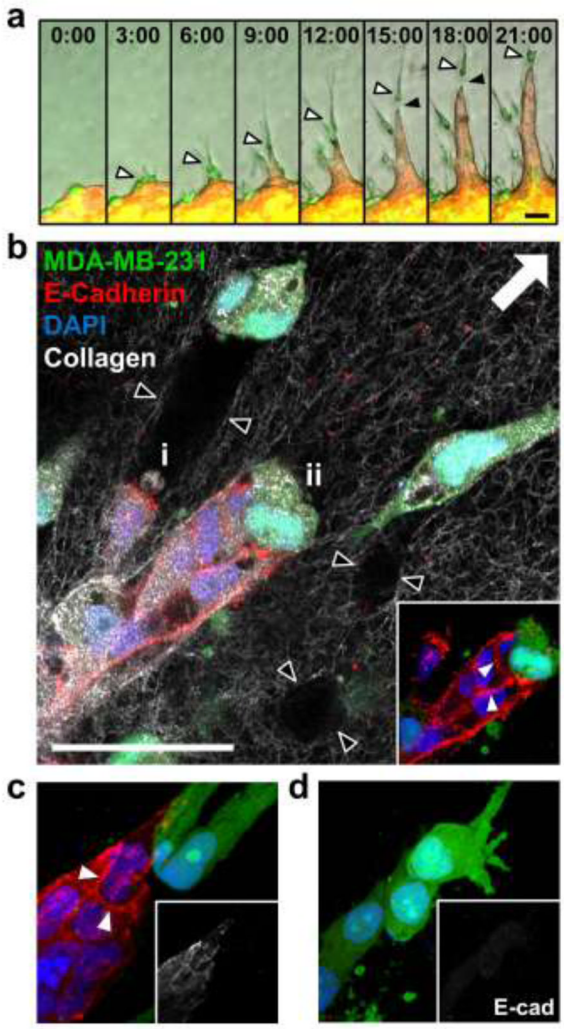

Fig. 6.

Intercellular interactions during co-invasion. **(a)** Time-lapse fluorescent and phase microscopy (10×) of a co-culture spheroid invading into 1.5 mg ml^{-1} collagen matrix. White arrowheads highlight MDA-MB-231 cell (green) leading an invasive strand of MCF-10A cells (red). Black arrowheads identify transient gap between leading MDA-MB-231 cell and following MCF-10A cells. Time shown indicates hours after embedding. **(b)** Single confocal section (40×) of multicellular spheroid composed of MCF-10A mammary epithelial cells and fluorescently-labeled MDA-MB-231 malignant breast cells (green) after 48 h of invasion into collagen matrix (white fibers). E-cadherin (red) and nuclei (DAPI; blue) were detected by confocal fluorescence microscopy. Inset highlights E-cadherin-positive cell-cell adhesions between MCF-10A cells (white arrowheads). Black arrowheads indicate boundaries of matrix microtracks generated by invading malignant leader cells. Two MCF-10A induced-invasion strategies are demonstrated: (i) MCF-10A cells fill matrix tunnels left by invading MDA-MB-231 cells; (ii) MCF-10A cells remain adjacent to leading MDA-MB-231 cells, but with no detectable E-cadherin-based adhesions between the two cell types. **(c, d)** Maximum intensity z-projections of invasive cellular strands from different regions of a co-culture spheroid demonstrate (c) an E-cadherin-positive (white arrowheads) cohort of MCF-10A cells following leading MDA-MB-231 cells and (d) lack of E-cadherin-positive cell-cell adhesions between adjacent singly invading MDA-MB-231 cells. Insets

highlight E-cadherin distribution. Arrow indicates direction of invasion away from spheroids for panels b-d. Scale bars = 50 μm

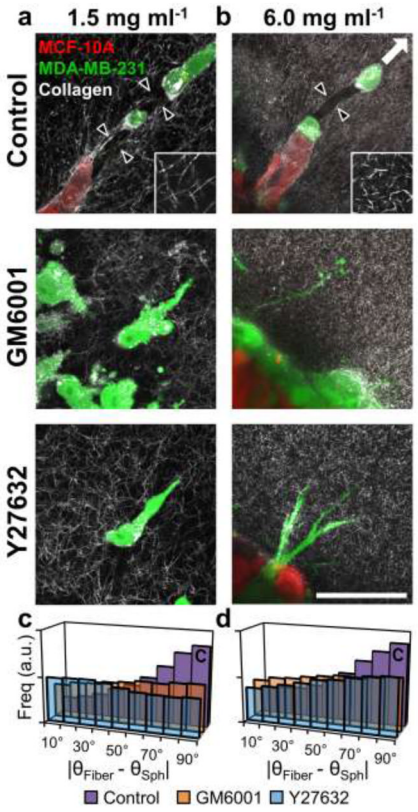

Fig. 7.

Effects of proteolysis and cell contractility on matrix reorganization during invasion. Confocal reflectance images (40×) of cells invading from co-culture spheroids into **(a)** 1.5 mg ml^{-1} or **(b)** 6.0 mg ml^{-1} collagen matrices under control conditions or treated with inhibitors of matrix metalloproteinases (GM6001; 20 μM) and ROCK (Y-27632; 10 μM). Images are single slices aligned parallel to the plane of invasion taken at the spheroid-matrix interface. Black arrowheads indicate boundaries of matrix microtracks generated by leading malignant cells. Insets are high-magnification (20μm × 20μm) images of 1.5 and 6.0 mg ml^{-1} collagen matrices to highlight fiber and pore microarchitecture. Quantification of collagen fiber orientation relative to the spheroid surface at the spheroid-matrix interface within **(c)** 1.5 mg ml^{-1} or **(d)** 6.0 mg ml^{-1} collagen matrices under control conditions (purple bars), MMP inhibition with GM6001 (orange bars), or ROCK inhibition with Y27632 (blue bars). Scale bar = 50μm

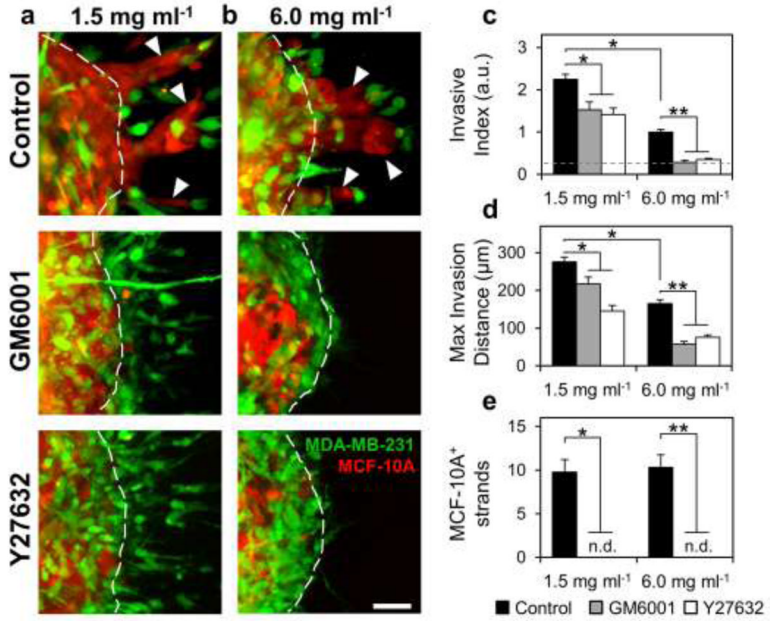

Fig. 8.

Role of proteolysis and cell contractility in induced collective epithelial cell invasion. Maximum intensity z-projections (10×) of co-culture multicellular spheroids embedded within **(a)** 1.5 mg ml^{-1} or **(b)** 6.0 mg ml^{-1} collagen gels and treated with GM6001 (20 μM) or Y-27632 (10 μM). Arrowheads indicate epithelial cell-containing invasive strands. Dashed lines indicate original spheroid boundaries. Quantification of **(c)** Invasive Index, **(d)** Maximal Invasion Distance, and **(e)** the incidence of MCF-10A-positive invasive strands under control conditions (black bars), GM6001 treatment (gray bars), and Y27632 treatment (white bars). Dashed gray line in (c) denotes Invasive Index of non-invasive epithelial monoculture spheroids. MCF-10A-positive invasive strands were not detected under GM6001 or Y27632 treatment (n.d.). * indicates statistical significance compared to control 1.5 mg ml^{-1} condition; ** indicates statistical significance compared to control 6.0 mg ml^{-1} condition. Scale bar = 50 μm